LASER INDUCED INTERMODULATED FLAME FLUORESCENCE: APPLICATION TO ANALYTICAL ATOMIC FLUORESCENCE

By

LUCAS P. HART, III

A DISSERTATION PRESENTED TO THE GRADUATE SCHOOL
OF THE UNIVERSITY OF FLORIDA IN
PARTIAL FULFILLMENT OF THE REQUIREMENTS
FOR THE DEGREE OF DOCTOR OF PHILOSOPHY

UNIVERSITY OF FLORIDA

1984

ACKNOWLEDGEMENTS

I should like to express my gratitude to my research director, Dr. James D. Winefordner for encouragement, patience, and persistence throughout the years I have worked with him. In addition, his dauntless energy and quest for new ideas serve as inspiration for those in his research group.

I should like to thank the postdoctoral associates and graduate students in his research group, past and present, for providing a stimulating environment with many interesting and educational diversions in the course of my work for this degree. Special thanks go to Dr. Nicolo Omenetto for challenging dialogue and continued encouragement.

Finally, I should like to express my thanks and appreciation to my parents for all their continuing support and understanding.

TABLE OF CONTENTS

Abstract of Dissertation Presented to the Graduate School of the University of Florida in Partial Fulfillment of the Requirements for the Degree of Doctor of Philosophy

LASER INDUCED INTERMODULATED FLAME FLUORESCENCE: APPLICATION TO ANALYTICAL ATOMIC FLUORESCENCE

By

Lucas P. Hart, III

April 1984

Chairman: James D. Winefordner
Major Department: Chemistry

Many transitions used in atomic flame fluorescence can be saturated with modern high power lasers. The fluorescence signal reaches a constant value as the laser irradiance is increased. If a cw laser is modulated, saturation of the transition will cause nonlinear response to the time-varying excitation waveform and generate harmonics in the fluorescence signal. If two laser beams are modulated at different frequencies and the two beams are combined, saturation of the transition will produce signals at the intermodulation product frequencies. Under saturation conditions, the signals at these frequencies may be a significant fraction of the signal at the fundamental frequency.

Scatter ,e.g., Rayleigh or Mie scatter, is a linear process and does not produce such additional frequencies.

Measurement at the intermodulation product frequency, under saturation conditions, may significantly reduce the effect of scatter upon the fluorescence signal measured at a resonance line. Additionally, the laser beam cross-sectional area can be made quite small (10^{-3} cm^2) so that the intermodulation resulting from two crossed, modulated beams may be a powerful tool for spatial diagnostics.

The intermodulation signal for Na in a premixed, laminar H_2-O_2-Ar flame has been studied using a cw dye laser. Strong intermodulation signals were observed. The interference from scatter of the laser beam was greatly reduced by measuring fluorescence at one of the intermodulation product frequencies.

CHAPTER ONE
INTRODUCTION

Laser induced fluorescence spectroscopy has become a valuable analytical tool in a wide variety of fields, now that lasers are readily available with wavelengths in the UV-visible region (1,2,3,4). It has the advantages of good sensitivity and spatial resolution. Lasers may be focused to beam diameters of only tens of micrometers, giving the potential for high spatial resolution measurements, or the use of micro-samples. Laser induced fluorescence has found use in ultra-trace analysis, where the goal may be single-atom detection (5). Concentrations as low as 10^4 atoms/cm^3 have been measured for sodium in atmospheric pressure flames (6). Various types of laser induced fluorescence have found application in combustion diagnostics (2,3,7), where techniques originally developed using atomic fluorescence of sodium have been extended to the measurement of concentrations of various radicals throughout the combustion process.

One type of fluorescence spectroscopy, which only became feasible with the availability of high power lasers, is saturation spectroscopy. In fluorescence, the signal is proportional to the excited state population. The excited

state may deactivate either radiationally or by collisional deactivation. Thus the collisional environment may affect the fluorescence signal. However, if the excitation beam intensity is high enough, the population of the upper level reaches a maximum as the rate of stimulated emission exceeds the rate of spontaneous emission or collisional deactivation. The saturation, as this condition is called, may be used to advantage in different ways. The fluorescence signal is determined by the upper-level population, which is now independent of the collisional environment, so saturation may be of value in diagnostic studies, where the collisional environment may change. For this reason, saturation spectroscopy has found extensive application in combustion diagnostics, where the interest is in radical concentrations throughout the combustion zone. If the two levels (considering a two-level system) have equal statistical weights, the upper level will have half the total population with full saturation. With saturation, the fluorescence signal for a given analyte density will also be a maximum. That is, since the maximum number of atoms are in the upper state, the fluorescence transition rate will also be maximum as the fluorescence transition rate is the upper level density times the spontaneous transition probability. In analytical atomic spectroscopy, saturation spectroscopy can be applied to ultra-trace analysis and in the quest for single-atom detection.

One practical limit to the sensitivity of laser induced fluorescence spectroscopy is scatter of the laser radiation (8), whether it be Rayleigh scatter from the flame gases, Mie scatter from particulates, or scatter from the sample cell. Several techniques have been used to avoid these effects. One of the most effective is to use non-resonance fluorescence (1), that is, to look at a different transition from the excited state to a lower state. This may not be practical, due to a lack of other transitions or a low transition probability. Advantage may be taken of the polarization of Rayleigh and Mie scatter, and polarizers used to reduce the scatter-to-signal ratio (8,9). Two light sources may be used, as in conventional background correction techniques, but with a large scatter signal and small fluorescence signal, statistical uncertainties may be large as the result of subtracting two large, uncorrelated numbers. Wavelength modulation of a cw dye laser has been used to correct for scatter resulting in an order of magnitude improvement over amplitude modulation (10).

Another approach, proposed by Alkemade (5,11), is a variant of the intermodulation technique originally applied to high-resolution spectroscopy by Sorem and Schawlow (12). In this approach, the laser beam is split into two beams of equal intensity, each is amplitude-modulated at a different frequency, and then the beams are passed through the atom cell in opposite directions, intersecting therein.

Different configurations are shown in Figure 1-1. The scatter will be proportional to the sum of the intensities of the two beams. Under conditions of full saturation, the peak fluorescence signal will be the same, independent of whether one or two beams are present. In this case, side-bands will be generated at frequencies equal to the sum and difference of the two modulation frequencies. This approach is similar to one evaluated by Freuholz and Gelbwachs (13), in which the laser beam is sinusoidally modulated; the fluorescence signal also appears at higher harmonics in the case of saturation.

In this work, the application of intermodulated fluorescence to atomic flame spectroscopy was considered. The system used for experimental characterization was a H_2-O_2-Ar flame, and a cw dye-laser to saturate sodium atomized in the flame. The behavior of sodium atoms in flames has been extensively investigated and documented (14). Sodium atoms are readily saturated by cw dye lasers. The cw dye laser is appropriate for investigation of the intermodulated fluorescence, as it is stable and easily modulated, which cannot be said of many higher powered pulsed lasers.

The characteristics of various optical configurations, e.g., single-beam modulation, double-beam modulation, tightly-focused laser beams, or beams defocused at the point of

Figure 1-1. Optical configuration for laser induced flame fluorescence saturation spectroscopy.

a) single-beam configuration for harmonic saturation
b) double-beam configuration with nearly co-linear beams for maximum intermodulation signal
c) double-beam configuration with crossed beams for high spatial-resolution intermodulation signal

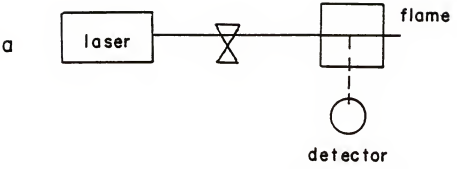
a
laser
flame
detector

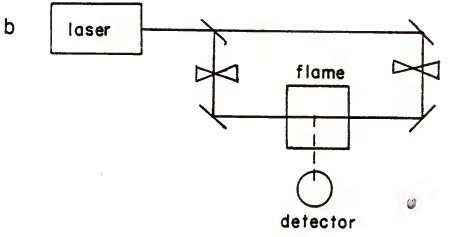
b
laser
flame
detector

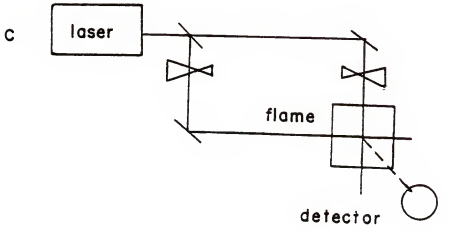
c
laser
flame
detector

observation, were studied to determine the range of application of the intermodulated technique. Real-time measurements using a phase-sensitive amplifier (lock-in amplifier) permitted the optimization of various parameters and were used to demonstrate the application of intermodulated fluorescence to analytical measurements. The fluorescence signals were also digitized, and power spectra calculated using a fast Fourier transform (FFT) to simultaneously determine the magnitudes of the signals at the various intermodulation products frequencies, in order to characterize the behavior of the intermodulated fluorescence signal.

A qualitative description of the behavior of the intermodulated fluorescence was derived using a basic model of a two-level atomic system, the rate equation approach to solving the steady-state system response, and Fourier series expansion of the time-varying modulation waveforms.

The significant reduction of scatter resulting from the use of an intermodulation product frequency for the fluorescence measurment was shown. An alternative application of intermodulated flame fluorescence, for spatial resolution, was demonstrated.

CHAPTER TWO
THEORETICAL CONSIDERATIONS

The theory of saturation spectroscopy has been well documented in detail for a wide range of applications, including high resolution atomic and molecular spectroscopy (15), optical pumping (16), and analytical spectroscopy (1). The intermodulated absorption signal has been treated, using several different formalisms. Freuholz and Gelbwachs have considered the case of single beam saturating atomic fluorescence in a flame (13). For this work, a simplified, i.e., two-level, system will be considered to show the origin of the intermodulated fluorescence signal, first for a single-beam system and then for a crossed-beam system. The two-level system is adequate to show the origin of the intermodulated component and show the relationship to the laser excitation. A quantitative analysis would have to take into account factors such as the Gaussian intensity distribution of the laser, laser induced chemistry and ionization, multiple electronic levels, etc. The rate equation approach used is appropriate for atmospheric pressure flames (17).

The case considered is an atom with two energy levels that is a trace constituent in an atmospheric pressure system where the collision rates are high enough for coherent

effects to be disregarded. The excitation source is considered to have a spectral profile much greater than the absorption profile of the absorbing atoms, and thus has a uniform spectral density and interacts with all the absorbing atoms. The source is also assumed to have a uniform spatial distribution. The two levels of the atomic system are assumed to have equal statistical weights. The source is tuned to the atomic transition, with a spectral bandwidth $\delta\nu$ (Hz), a power Φ (W), and a cross-section S (cm^2). The population of the levels (cm^{-3}) is indicated as n_1 and n_2 and the total atom population ,$n_1 + n_2$, as n_T.

Using a rate equation approach, and ignoring collisional excitation, as shown in Fig. 2.1a, the population of the two levels is given by

$$n_1[B_{12}E_\nu/c] = n_2[B_{21}E_\nu/c + A_{21} + k_{21}] \qquad (2.1)$$

where:

B = $(c^3/8\pi h\nu^3\tau_{sp})$: Einstein coefficient for stimulated absorption and emission, $J^{-1}cm^3Hz$;

A = Einstein coefficient for spontaneous emission, s^{-1};

k = collisional rate constant, s^{-1};

c = light velocity in vacuum, cm s^{-1};

h = Planck constant, J s;

ν = resonance frequency of the transition, Hz;

τ_{sp} = spontaneous (radiative) lifetime of the upper level, s ($\equiv 1/A$);

τ = lifetime of upper level (including collisions) s ($\equiv 1/A+k$);

$E_\nu = \frac{\Phi}{\delta\nu S}$ = spectral irradiance of the laser beam, $J\ s^{-1}\ cm^{-2}\ Hz^{-1}$;

The saturation parameter or saturation irradiance, E^s, is defined as that irradiance which would give an upper-level population half that of an infinite irradiance (1). Then,

$E^s_\nu = \frac{8h\nu^3}{2c^2\tau}\tau_{sp}$ = saturation parameter for the atomic transition, $J\ s^{-1}cm^{-2}Hz^{-1}$.

Substituting both the saturation parameter, E^s_ν, and $n_T - n_2$ for n_1 in Eqn. 2.1 gives:

$$\frac{n_2}{n_T} = \frac{1}{2}\,\frac{E^o_\nu}{E^s_\nu + E^o_\nu} \tag{2.2}$$

This is the steady-state approximation; the relative populations of the two levels are shown in Fig. 2.1b. If the atomic relaxation time is fast compared to the modulation rate, the time-varying excited-state population is given by

$$\frac{n_2(t)}{n_T} = \frac{1}{2}\,\frac{E_\nu(t)}{E^s + E_\nu(t)} \tag{2.3a}$$

or

$$\frac{n_2(t)}{n_T} = \frac{1}{2}\,\frac{E^o_\nu f(t)}{E^s + E^o_\nu f(t)} \tag{2.3b}$$

where $E_\nu(t)$ is the time varying spectral irradiance, E^o_ν the peak spectral irradiance, and f(t) the function describing the time variation. The fluorescence radiance is

$$B_F = n_2 h\nu\ (\ell/4\pi)A_{21} \tag{2.4}$$

where ℓ(cm) is the depth of the fluorescence volume. The

Figure 2-1. Two-level system

a) energy-level diagram

B = Einstein coefficient for stimulated absorption and emission

A_{21} = Einstein coefficient for spontaneous emission

k_{21} = collisional quenching rate constant

b) Saturation curve for two-level system

n_2, n_1 = population density of levels two and one

E_ω = source spectral irradiance

E_υ = saturation irradiance

a)

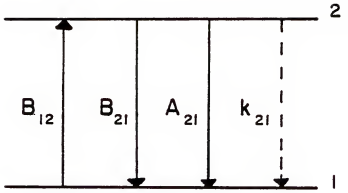

b)

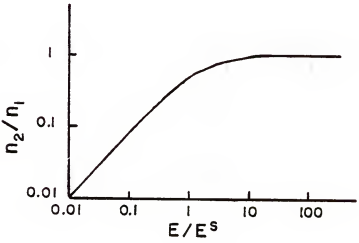

time-varying fluorescence signal is thus proportional to $n_2(t)$. The effect of varying source irradiance will be examined for single-beam excitation, with arbitrary waveform, and crossed or co-linear beams with square-wave or sinusoidal modulation.

Single-Beam Modulation

Considering the amplitude-modulated excitation waveform as a 100% modulated positive periodic function, it may be expressed as

$$E_\nu(t) = \frac{E_\nu^o}{2}[1+f(t)] \tag{2.5}$$

where E_ν^o is the peak irradiance and $f(t)$ could be $\sin(\omega t)$ for sinusoidal modulation for example. To simplify the notation in the following treatments, let $y(t) = 2(n_2/n_T)$. Then the equation (2.3b) may be rewritten as

$$y(t) = \frac{E_\nu^o\ [1+f(t)]}{2E_\nu^s + E_\nu^o[1+f(t)]} \tag{2.6}$$

or

$$y(t) = \frac{E_\nu^o\ [1+f(t)]}{2E_\nu^s + E_\nu^o + E_\nu^o f(t)} \tag{2.7}$$

Since $2E_\nu^s + E_\nu^o + E_\nu^o f(t)$ is equivalent to

$$[2E_\nu^s + E_\nu^o][1 + \frac{E_\nu^o}{2E_\nu^s + E_\nu^o}\ f(t)] \tag{2.8}$$

equation 2.7 may be written as

$$y(t) = \frac{E_\nu^o[1+f(t)]}{2E_\nu^s + E_\nu^o}\left[\frac{1}{\{1+\frac{E_\nu^o f(t)}{2E_\nu^s + E_\nu^o}\}}\right] \tag{2.9}$$

Let $\alpha = E_\nu^o/2E_\nu^s+E_\nu^o$ and $z = \alpha f(t)$. Since $|z|<1$, a power series expansion may be used (18), i.e.,

$$(1+z)^{-1} = 1 - z + z^2 - z^3 + \ldots\ldots \tag{2.10}$$

and

$$y(t) = \left(\frac{E_\nu^o[1 + f(t)]}{2E_\nu^s + E_\nu^o}\right)(1-z+z^2-z^3 + \ldots.) \tag{2.11}$$

The effect of saturation upon the response of y(t) to the modulation waveform may be examined by substituting for f(t).

Sinusoidal Modulation

In this case, f(t) may be represented as either $\sin(\omega t)$ or $\cos(\omega t)$. Keeping terms with frequency up to a power of three

$$y(t) = \left(\frac{E_\nu^o}{2E_\nu^s + E_\nu^o}\right)\{1 + (1-\alpha)[f(t)-\alpha f^2(t) + \alpha^2 f^3(t)]\} \tag{2.12a}$$

gives

$$y(t) = \frac{E_\nu^o}{2E_\nu^s + E_\nu^o}\{1 + (1-\alpha)[\cos\omega t - \tfrac{1}{2}\alpha(1+\cos 2\omega t) + \tfrac{1}{4}\alpha^2(\cos\omega t+\cos 3\omega t)]\} \tag{2.12b}$$

It can be seen that the effect of increasing α is to decrease the fraction of the total signal with a frequency component the same as the modulation frequency, and to increase the harmonic content.

Square-Wave Modulation

A square wave may be represented as a Fourier series (19)

$$f(t) = \frac{2}{\pi}(\cos\omega t - \frac{1}{3}\cos 3\omega t + \frac{1}{5}\cos 5\omega t \ldots\ldots) \qquad (2.13)$$

From (2.12a), it can be seen that the frequency components of the original excitation waveform are attenuated. To determine the resultant frequency components, the second power term may be examined. The $(1-\alpha)\alpha f^2(t)$ may be expanded, keeping terms up to the 5th harmonic

$$f^2(t) = [\frac{2}{\pi}(\cos\omega t - \frac{1}{3}\cos 3\omega t + \frac{1}{5}\cos 5\omega t)]^2 \qquad (2.14a)$$

$$= \frac{4}{\pi^2}(\cos^2\omega t - \frac{1}{3}\cos 3\omega t\cos\omega t + \frac{1}{5}\cos 5\omega t\cos\omega t - \frac{1}{3}\cos\omega t\cos 3\omega t + \frac{1}{9}\cos 3\omega t\cos 3\omega t - \frac{1}{15}\cos 5\omega t\cos 3\omega t + \frac{1}{5}\cos\omega t\cos 5\omega t - \frac{1}{15}\cos 3\omega t\cos 5\omega t + \frac{1}{25}\cos 5\omega t\cos 5\omega t) \qquad (2.14b)$$

Since $\cos(A)\cos(B) = 1/2(\cos(A+B)+\cos(A-B))$, this may be expressed as

$$f^2(t) = \frac{2}{\pi^2}[1+\cos 2\omega t - \frac{1}{3}(\cos 2\omega t+\cos 4\omega t) + \frac{1}{5}(\cos 4\omega t+\cos 6\omega t) - \frac{1}{3}(\cos 2\omega t+\cos 4\omega t) + \frac{1}{9}(1+\cos 6\omega t) - \frac{1}{15}(\cos 2\omega t+\cos 8\omega t) + \frac{1}{5}(\cos 4\omega t+\cos 6\omega t) - \frac{1}{15}(\cos 2\omega t+\cos 8\omega t) + \frac{1}{25}(1+\cos 10\omega t) \qquad (2.14c)$$

Continuing the expansion of this series gives coefficients of 1, -1/3, -1/15, -1/35, -1/63, -1/99 or a second harmonic term

$$f^2(t) \simeq (1/\pi^2)\cos 2\omega t$$

Since 2.14c contains only even terms, it can be seen that the the third-power term will have no second harmonic term, while the second-harmonic terms from the fourth-power term have a coefficient of $\alpha^2/4$ and will be smaller. The ratio of the second harmonic to the fundamental is then approximately $\alpha/2\pi$.

Double-Beam Modulation

The effect of modulating two intersecting beams at different frequencies may be examined using the same approach as for the single-beam case, but first, a heuristic approach to the square-wave modulation more clearly illustrates the effects, and gives an estimate of the coefficients for the intermodulated terms.

Square-Wave Modulation

In Figure 2-2, the first two waveforms are those of the excitation waveforms. If there is linear combination, or superposition, of the two waves, the amplitude will be the sum of the two, giving a result as in Fig. 2.2c. In the case of intermodulation, or nonlinear response, the amplitude of the resulting waveform may be less than the sum of the two waves, as in Fig 2.2d. The analysis of the intermodulation process is considerably simplified by considering the resultant waveform as being the superposition of the train of square waves in (a) and modulated train of waves with frequency of (b). The modulated train may be expressed

Figure 2-2. Waveforms for intermodulated fluorescence $_1y_o$
a) square-wave modulation of beam 1, amplitude $_1y_o$
b) square-wave modulation of beam 2, amplitude $_2y_o$
c) linear combination of a and b waveforms
d) saturation, non-linear combination of a and b
e) modulation waveform, when multiplied by waveform in b and added to waveform in a, gives d

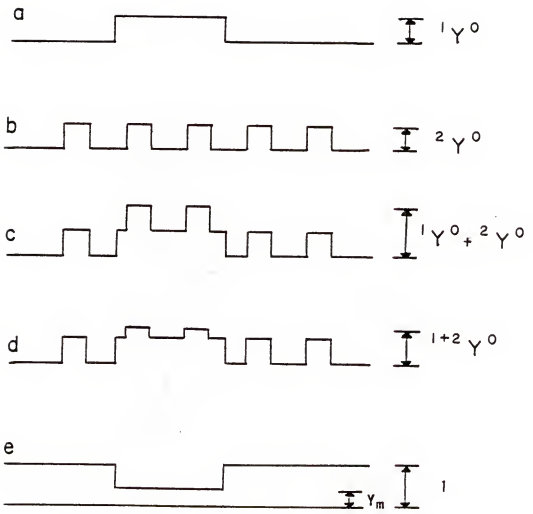
a
$^1Y^0$
b
$^2Y^0$
c
$^1Y^0 + ^2Y^0$
d
$^{1+2}Y^0$
e
Y_m
1

as the product of the train in (b), $^{2}y(t)$, and a modulation function, M(t), i.e.,

$$^{1+2}y(t) = {}^{1}y(t) + {}^{2}y(t)M(t) \tag{2.15}$$

The modulation function, M(t) shown in (e), has the same frequency as the wavetrain in (a), and an amplitude varying between 1 and y_m, where

$$y_m = \frac{^{1+2}y^o - {}^{1}y^o}{{}^{2}y^o}$$

and $^{1+2}y^o$ is the amplitude when both beams are combined. For the case of square-wave modulation being considered, the time-varying functions may be expressed as

$$^{1}y(t) = \frac{^{1}y^o}{2}[1+f_1(t)] \tag{2.16a}$$

$$^{2}y(t) = \frac{^{2}y^o}{2}[1+f_2(t)] \tag{2.16b}$$

The modulation function may be expressed as

$$M(t) = \frac{1}{2}[(1+\frac{^{1+2}y^o - {}^{1}y^o}{{}^{2}y^o} + (1-\frac{^{1+2}y^o - {}^{1}y^o}{{}^{2}y^o})f_1(t)] \tag{2.16c}$$

The square-wave function may be represented by the Fourier series expansion (eqn. 2.13). Keeping only those terms with the fundamental frequency in each term, we get for the intermodulation term, $y_{im}(t)$

$$y_{im}(t) = \frac{2}{\pi^2}(^{1}y^o + {}^{2}y^o - {}^{1+2}y^o)\cos\omega t\cos\omega t \tag{2.17}$$

The height of the square wave, with a given excitation,

i.e., ${}^1y^o$, ${}^2y^o$, or ${}^1y^o+{}^2y^o$ may be determined from the basic relationship, Eqn. 2.2. After algebraic manipulation, the amplitude of intermodulation product may be expressed in terms of the excitation amplitudes ($y_{im}(t) = C_{im}f(t)$) as

$$C_{im} = \frac{1}{\pi^2}\left(\frac{{}^1E_\nu^o}{{}^1E_\nu^o+E_\nu^s} + \frac{{}^2E_\nu^o}{{}^2E_\nu^o+E_\nu^s} - \frac{{}^1E_\nu^o+{}^2E_\nu^o}{{}^1E_\nu^o+{}^2E_\nu^o+E_\nu^s}\right) \tag{2.18}$$

From examination of this equation, it is apparent that at low intensities, i.e., ${}^1E_\nu^o$ or ${}^2E_\nu^o \ll E_\nu^s$, the intermodulated term goes to zero. At high intensities, ${}^1E_\nu^o, {}^2E_\nu^o \gg E_\nu^s$, C_{im} goes to $1/\pi^2$. For a given laser power, the maximum intermodulation signal is obtained if the power is divided equally between the two beams, in which case

$$C_{im} = \frac{1}{\pi^2}\left[\frac{(E_\nu^o)^2}{(E_\nu^o+E_\nu^s)(2E_\nu^o+E_\nu^s)}\right] \tag{2.19}$$

where the peak intensity E_ν^o is the same for either beam, i.e., $E_\nu^o = {}^1E_\nu^o = {}^2E_\nu^o$. Since the component at either fundamental,in the lack of the other beam being on, is given by equations 2.13 and 2.16, the ratio of the component at the intermodulation frequency to that at the fundamental (one beam blocked so there is no intermodulation) is

$$\frac{C_{im}}{C^o} = \frac{1}{\pi}\,\frac{E_\nu^o}{2E_\nu^o + E_\nu^s} \tag{2.20}$$

It should be noted that this is a first-order approximation. Intermodulation terms as a result of the fundamental and

third harmonic term of the Fourier series expansion of the modulation waveform will give components at $(3\omega_1 + \omega_2)$, $(3\omega_1 - \omega_2)$, $(\omega_1 + 3\omega_2)$, and $(3\omega_2 - \omega_1)$, each with a coefficient one-sixth that of the intermodulation term resulting from the fundamentals only. This heuristic approach gives a simple presentation based upon square-wave modulation. For an arbitrary waveform, an analysis similar to that for the single-beam system can be performed.

Arbitrary Waveform Modulation

For an arbitrary waveform, the basic equations used for the single-beam case may be expanded for the case of two crossed or nearly co-linear beams modulated at different frequencies. The instantaneous intensity will be the linear sum of the intensities of each of the beams and Eqn. 2.5 becomes

$$E_\nu(t) = \frac{1E_\nu^o}{2}[1 + f_1(t)] + \frac{2E_\nu^o}{2}[1 + f_2(t)] \qquad (2.21)$$

These equations only apply to 100% modulation of each beam. A more general treatment would include a possible offset in the dc term as was done for the modulation waveform in the two-beam square treatment (Eqn. 2.16c). For clarity and ease of notation, only 100% modulation will be discussed. Following the same algebraic steps used in the single-beam case, the time-varying population of the upper level may be written

$$y(t) = \frac{{}^1E_\nu^o[1+f_1(t)] + {}^2E_\nu^o[1+f_2(t)]}{[2E_\nu^s+{}^1E_\nu^o+{}^2E_\nu^o][1+\frac{{}^1E_\nu^o}{2E_\nu^s+{}^1E_\nu^o+{}^2E_\nu^o}f_1(t) + \frac{{}^2E_\nu^o}{2E_\nu^s+{}^1E_\nu^o+{}^2E_\nu^o}f_2(t)]} \quad (2.22)$$

This is similar to Eq. 2.9. Using the series expansion, where now

$$z = \frac{{}^1E_\nu^o}{2E_\nu^s+{}^1E_\nu^o+{}^2E_\nu^o}f_1(t) + \frac{{}^2E_\nu^o}{2E_\nu^s+{}^1E_\nu^o+{}^2E_\nu^o}f_2(t) \quad (2.23)$$

we obtain a general equation for the two-beam case, modulated at different frequencies

$$y(t) = \frac{1}{2E_\nu^s+{}^1E_\nu^o+{}^2E_\nu^o}\{{}^1E_\nu^o[1+f_1(t)]+{}^2E_\nu^o[1+f_2(t)]\}[1-z+z^2+\ldots] \quad (2.24)$$

To compare this to the previous treatment of the square-wave modulated two-beam system, consider the fundamental frequency only of the square wave as before, the first power term of the power series expansion, and let $E_\nu^o={}^1E_\nu^o={}^2E_\nu^o$. Equation 2.24 then simplifies to

$$y(t) = \frac{E_\nu^o}{E_\nu^s+E_\nu^o}[1 + \frac{2}{\pi}(\cos\omega_1 t+\cos\omega_2 t)][1-z] \quad (2.25)$$

which gives an intermodulation coefficient of

$$C_{im} = \frac{1}{\pi^2}\left(\frac{E_\nu^o}{E_\nu^s + E_\nu^o}\right)^2 \quad (2.26)$$

This result is quite similar to that obtained in Eq. 2.19. Thus both approaches give the same qualitative results, showing how the intermodulation component originates. The first treatment of square-wave modulation for the two-beam system is conceptually simpler; the more general approach, based on an arbitrary waveform, can be extended to compare the effects of varying degree of modulation, different waveforms, and real conditions which have been avoided in the simplified model used here, e.g., the effects of Gaussian spatial intensity distribution could be included and the appropriate equations numerically solved.

CHAPTER THREE
EXPERIMENTAL EQUIPMENT AND METHODS

The experimental system used for fluorescence measurements is schematically illustrated in Figure 3-1. It may be functionally broken down into the optical system, for exciting and detecting the fluorescence, the atom cell, i.e., the flame, and the electronic detection and signal processing equipment. These will be discussed separately, and then the experimental procedures described.

Optical System

The principal optical system components and their manufacturers are given in Table 3-1. A continuous-wave dye laser, pumped by an argon-ion laser, was used as the excitation source. The theory of dye lasers and their application to analytical spectroscopy has been extensively discussed in numerous review articles and books (1,20,21,22); only the relevant characteristics will be discussed here. The Ar-ion laser has a nominal maximum output power of 18 W when operated in the all-lines mode. In this mode, a broad-band mirror is used as the rear reflector of the laser cavity, and lasing occurs simultaneously at the wavelengths of several different argon ion lines, primarily those with wavelengths of 514.5 nm and 488.0 nm. An alternative,

Table 3-1. Optical Equipment used in Intermodulated Fluorescence Studies and Its Source of Manufacture

Item	Source
Argon ion laser, Model 171-19	Spectra-Physics Mountain View, Calif.
CW dye laser, Model 375	Spectra-Physics
Power meter, Model 210	Coherent Radiation Palo Alto, Calif.
Beamsplitter, cube	Melles Griot Irvine, Calif.
Lenses, spherical achromatic doublets	Melles Griot
Lens positioner, 5-axis, Model LP-1	Newport Corporation Fountain Valley, Calif.
Lens, spherical biconcex	ESCO Products, Inc. Oak Ridge, N.J.
Polarizers, Glan Thompson	Karl Lambrecht Corp. Chicago, Ill.
Polarizer rotators, Model 1641	Oriel Corporation Stamford, Conn.
Chopper, Model 7500	Rofin-Math Associates Great Neck, N.Y.
Chopper, Model 125	Princeton Applied Research Corp., Princeton, N.J
Flame, burner head	laboratory-constructed
Nebulizer,mixing chamber, Model 303	Perkin-Elmer Norwalk, Conn.
Monochromator, Model H-10	American ISA Inc. Metuchen, N.J.
Photomultiplier, Model R777	Hamamatsu Middlesex, N.J.

single-line operation, uses a wavelength-selective element, namely a prism in front of the rear reflector. Higher output powers are obtained for a single line, than in the all-lines mode, but the total power is less. For pumping Rhodamine 6G, the dye used here, the all-lines mode gives more efficient conversion of argon ion laser pump power to dye laser output power. The power of the Ar-ion laser was monitored with the power meter included with the power supply. The power supply has two possible modes of operation: constant current or constant output, in which a feedback circuit is used to vary the current to maintain a constant output power. Adequate stability of the dye laser output was maintained using the constant current control and the constant output mode was not used.

The continuous-wave dye laser used had been modified with the extended cavity option (Spectra-Physics Model 341) for alternative use as a source of picosecond duration laser pulses. The output mirror for that option is not optimum for use for cw excitation, having a different focal length and transmission. Therefore, the conversion efficiency was lower than would normally be obtained with Rhodamine 6G. The argon-ion laser was operated to produce 9 W pump power, all-lines, which produced 1.4 W at the 589.6 nm wavelength of the sodium absorption line, using approximately 3 mM Rhodamine 6G (Exciton Rhodamine 590) in reagent-grade ethylene glycol. Typically, Rhodamine 6G has a conversion

efficiency of 25%. The Lyot or birefringent filter used as a wavelength tuning element in the dye laser results in a linewidth of approximately 80 pm (manufacturer's literature), which is large compared to the typical atomic absorption linewidths in flames of 5 pm (23), so that this laser may be considered a quasi-continuum source. The dye laser uses a free-flowing dye jet resulting from pumping the dye solution through a small nozzle at high pressures. The recommended operating pressure is that at which the power levels off as the pressure is increased. For this work, a pressure of 100 psig was used. (Pressures somewhat higher than that, e.g., above 120 psig, may cause the magnetically coupled pump to decouple, resulting in loss of pressure and possible splattering of dye over the optics, or the nozzle to come free of its holder, ending up in the dye reservoir, and resultant loss of lasing.)

Optical Components

Low-loss dielectric mirrors were used for steering the beam from the cw dye laser to the flame system. As indicated in Figure 3-1, a beamsplitter was used for measurements involving two beams. The beamsplitter was a cube type beamsplitter, composed of two right angle prisms, with a metal-dielectric film deposited on the interface before they are cemented together. The percentage transmittance and reflectance are specified as 45 and 55, respectively; however, this does not account for losses as a result of the

Figure 3-1. Experimental system for intermodulated flame fluorescence. Symbols for equipment are

BS beam splitter
CH chopper
f_1+f_2 lock-in reference circuit
M mirror
L lens
PMT photomultiplier

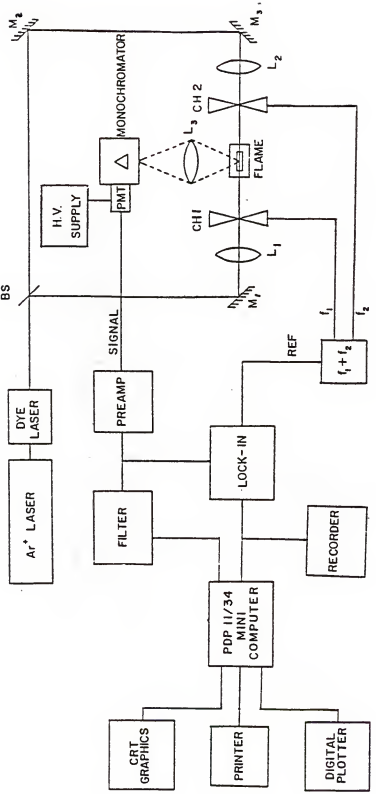
M_2
M_3
L_2
MONOCHROMATOR
L_3
CH 2
FLAME
H.V. SUPPLY
PMT
CH1
L_1
BS
M_1
SIGNAL
REF
f_1
f_2
f_1+f_2
DYE LASER
PREAMP
Ar⁺ LASER
LOCK-IN
FILTER
RECORDER
PDP 11/34 MINI COMPUTER
CRT GRAPHICS
PRINTER
DIGITAL PLOTTER

metal-dielectric film. The transmittance and reflectance were measured to be 37% and 53%. Single beam measurements were made with the beamsplitter removed and only the beam path on the right of the diagram (M2, M3, L2, CH2) used.

For all dye laser output power measurements, a Coherent absorption type power meter, with a sensitivity of 1 mV/W was used, in conjunction with the Coherent readout, or a microvoltmeter (Boonton model 95A) and recorder readout.

Achromatic doublet lenses with a focal length of 300 mm were used to focus the laser into the flame. Assuming a Gaussian spatial distribution and the measured divergence of 2 mrad for the dye laser, the cross-sectional area of the waist of the focused beam is calculated to be of the order of 10^{-3} cm^2. Because of the critical positioning required for alignment of the two beams with respect to each other, five-axis lens positioners, with fine adjustment screws allowing better than 1 μm resolution, were used. The choppers were placed as close to the flame as space would permit so that the wave form of the modulated laser beam would be as close to a square wave. The Rofin chopper (CH1) was operated at 178 Hz, and had a 9 mm aperture in the rotational direction. The PAR chopper (CH2) was operated at 260 Hz and had a 15 mm aperture in the rotational direction. (Both had blades with fan-blade shaped apertures.)

Flame System

A nearly-stoichiometric H_2-O_2-Ar flame was supported on a laboratory constructed Meeker type burner, which has been used extensively in this laboratory for flame diagnostic studies (24). The brass burner head has 96 holes, in a 8x12 rectangular grid, 32 for the inner flame in which the sample is atomized, and 64 for the outer flame which served to keep the inner flame composition and temperature uniform. The inner flame cross section was approximately 4 mm by 8 mm. The burner head was mounted on a standard premixing chamber and pneumatic nebulizer . The gas flow rates were estimated to be 4.5, 2.3, and 9 L/min of hydrogen, oxygen and argon respectively. Another 2 L/min of argon were required for the nebulizer, which aspirated 2 mL/min. All measurements were made with the optical axis 2 cm above the burner top. All fluorescence measurements were made using a sodium concentration of 1 μg/mL.

For a similar flame, van Calcar, et al. (23) calculated and measured the saturation parameter for sodium; they measured a value of 5.6×10^{-20} J $cm^{-3} Hz^{-1}$, in terms of spectral volume density, (ρ_ν^s), which differed from the calculated value by less than the experimental error. For the laser used here, with a spectral bandwidth of 60 gHz, that value corresponds to a saturation parameter, in spectral irradiance, of about 100 W cm^{-2} ($E_\nu^s = \rho_\nu^s c \delta\nu$). Using a value of 10^{-3} cm^2 for the cross-sectional area of the beam waist,

a maximum irradiance of 1.2 kW cm^{-2} can be calculated; thus, the transition should be readily saturated.

Optical Detection System

Fluorescence was collected by a 2 in diameter, 2-1/2 in focal length lens (L3) and focused on the entrance slit of the high luminosity f/3.5 monochromator. An aperture was placed in front of the lens to reduce stray light. The monochromator was oriented vertically, with the slits parallel to the laser beam, to increase the volume of the intersecting laser beams that was viewed. The mimimum slit height of 2 mm was used. The 0.5 mm slit width used gave a spectral bandwidth of 4 nm, wide enough so both the 589.0 and 589.6 nm sodium lines were detected. The photomultiplier was operated at -600 V to keep the output current level below 10 μA and avoid nonlinear response of the photomultiplier tube.

Electronic Measurement System

Two different systems were used for measurements; the components are given in Table 3-2. A lock-in based system was used for real-time measurements. The results of making adjustments in the optical path, tuning the laser, etc. were followed using this system as were quantitative measurements after the system was adjusted. The computer-based digital data acquisition system was used to measure power spectra, so that the amplitudes of signals at the various

Table 3-2. Electronic Equipment used in Intermodulated Fluorescence Studies and Its Source of Manufacture

Item	Source
High voltage power supply, Model 226	Pacific Precision Measurements Concord, Calif.
Preamplifier, Model 113	Princeton Applied Research Corp., Princeton, N.J.
Lock-in amplifier, Dynatrac 391	Ithaco Inc. Ithaca, N.Y.
Lock-in reference	laboratory-constructed (Appendix A)
Recorder, dual pen, Series 5000	Houston Instruments Austin, Texas
Anti-aliasing filter	laboratory-constructed (Appendix A)
Minicomputer, PDP 11/34A	Digital Equipment Corporation Maynard, Mass.
Analog/digital converter, Model LPSAD-12	Digital Equipment Corporation
Video graphics display, GT600 option for DEC VT100	MATROX Electronic Systems Ltd. Quebec, Canada
Printer, Model IDS-445	Integral Data Systems, Inc. Milford, N.H.
Plotter, HiPlot DMP-4	Houston Instruments
Voltmeter, DC, Model 95A	Boonton Electronics Corp. Parsippany, N.J.

harmonics and intermodulation frequencies could be determined simultaneously. The analog system was used to monitor the signal to make sure there was no unusual change in signal during the digital data acquisition period. The voltage signal measured by each was generated by passing the current from the photomultiplier through a 10kΩ load resistor. That voltage was amplified by the preamplifier, normally with a gain between 10 and 200. The lower cutoff frequency of the preamplifier was set at 0.03 Hz to avoid DC drift problems, and the upper cut-off frequency set at 3 kHz to attenuate noise and also the higher harmonic components of the square wave modulated signal. The output of this preamplifier went to both the analog and the digital acquistion systems.

Analog Data Acquisition

The signal was processed by the lock-in amplifier. The output went to a scaler (designed by Dr. E. Voigtman of this research lab) which acted as an active divider for scaling the 10 V output for both the recorder and the 1 V input of the digital data system which was used for analyzing the statistics of the analog output.

The reference signal was generated from the reference signals from the two choppers. A logic circuit was constructed so that either chopper frequency could be selected, or the frequency of the sum or difference of the two frequencies (Appendix A). It was found that the FFT of the output from the exclusive OR circuit gave only the sum and

difference frequencies when the reference signals from both choppers were combined; the frequency components of each of the single-beam waveforms were suppressed. This simple circuit was followed by a high-Q frequency selective amplifier which generated a bipolar sinusoidal reference signal from the rectangular input signal. This frequency of this amplifier was adjusted to be that of the desired reference, i.e., f_1, f_2, or f_1+f_2. The second harmonic signal could be easily measured; the lock-in reference mode selector was switched to the 2f mode, and the phase readjusted for maximum signal.

For the single beam measurements, the power meter was placed in the position of chopper 1, so that the laser intensity could be continuously monitored. The ouput of the microvoltmeter went to another channel of the scaler. From there, after scaling, it went to the second channel of the recorder, and could also be sent to the digital data analysis system.

Digital Data Acquisition and Signal Processing

The computer system was used for digital data acquisition and processing using a fast Fourier transform program to calculate the power spectra which gave the amplitude of the various frequencies composing the signal. When using the fast Fourier transform (FFT), there was a trade-off between resolution, frequency range, processing time, and memory requirements. The frequency of the PAR chopper could

be varied, by changing the pulley ratio or the chopper wheel. The Rofin chopper frequency could be electronically varied continuously from several Hz to about 1 kHz. The frequency of the PAR was fixed at 280 Hz, and the Rofin arbitrarily set at 178 Hz. This gave a range of frequencies of interest from about 100 Hz (f_1-f_2) to about 500 Hz (f_1+f_2). The sampling frequency should be at least twice the highest frequency of interest (the Nyquist frequency) so that a sampling frequency of at least 1 kHz was required.

Since the signals were square wave modulated, the higher harmonics were present and would fold over if the sampling frequency were only twice the modulation frequency. In order to attenuate the higher harmonics, a fourth-order low-pass Butterworth filter was built (Appendix A). With the cut-off frequency set at 700 Hz, there was no significant attenuation of signals below 500 Hz. A sampling frequency of 4 kHz was selected so that the effect of the filter could be observed, and possible aliasing or fold-over minimized. A 1024-point transform gave 2 Hz resolution which was adequate to resolve the various frequency components of the intermodulated signal. The power spectrum analysis program (Appendix B), including the FFT, was based upon one recommended by the Digital Signal Processing Committee of the IEEE Acoustics, Speech, and Signal Processing Society (25). For the digital analysis, 8192 data points were acquired in real time, at the 4 kHz sampling rate, and

stored on disc. A Hamming window of 512 points was used to reduce side lobes, and the modified periodograms averaged. A single 1024-point FFT took about 4 s, or about one minute to perform one analysis (an average of 16 FFTs). The resulting power spectrum could be printed out, or plotted either using either frequency versus rms amplitude/$Hz^{1/2}$ or versus log power/Hz.

Experimental Methods

Single-Beam Measurements

For initial characterization of the system before going to the intermodulated measurements, a series of measurements were made using only the single-beam configuration mentioned above. By not using the beamsplitter, approximately 1.2 W (over the laser spectral bandwidth) could be delivered to the flame cell which should result in a higher degree of saturation. Two sets of measurements were made. The first, with constant power, but variable spot size, resulted from adjusting the lens (L2) so that the beam was defocused. Thus the volume of the flame illuminated changed as the lens was moved from the distance equal to the focal length.

In the second set, the spot size was kept nearly constant. Here one of the polarizers was placed in the excitation side (between M2 and M3). The power meter was placed at the position of the other chopper (CH1) so that the focused beam was smaller than the aperture of the power

meter. The laser was vertically polarized as a result of the optics of the dye laser cavity (both the dye stream and the birefringent filter were at Brewster's angle with respect to the laser beam). The power could be varied continuously by rotating the polarizer from an orientation parallel to the incoming light to perpendicular, which gave almost complete extinction. The power was varied from a maximum of 1.2 W to 2 mW and the fluorescence of the 1 ppm Na solution measured. The amplitude of the signal at the fundamental and harmonics was determined from the power spectra.

Two-Beam Measurements

After the single-beam measurements had been made, the beamsplitter was mounted and several series of measurements performed to evaluate the two-beam intermodulation scheme. The nearly co-linear configuration shown in Fig. 3-1 was used so that there would be maximal overlap between the two beams. An alternative would have been to have the beams crossing at an angle closer to 90^{o} than 180^{o}. This would have made alignment even more critical and resulted in a much smaller volume where intermodulation could occur. Two separate cases of the co-linear configuration were considered: one, with the beams tightly focused,and the other, having the beams defocused in the intersecting volume.

Tightly-focused beam alignment

For these measurements, the point of tightest focus was chosen. The procedure for determining that point was quite simple. One chopper frequency was selected as the reference. The laser beam was first coarsely focused by moving the lens positioner back and forth, along the optical rail, so that the narrowest portion of the beam appeared to be in the center of the flame. The fluorescence signal at the chopper frequency was then used as an indication of the alignment. The beam was moved vertically using the vertical adjustment of the 5-axis lens positioner. The point of maximum signal was taken to be the optical axis. The lens could then be moved along this axis using the translator of the lens positioner (0.25 in travel). For this adjustment, the minimum signal indicated the best focus, as a smaller fluorescence volume was illuminated, and the signal was saturated. (Changing the vertical adjustment would further decrease the signal, but that would be off the optical axis.) Either the fundamental or the second harmonic signal could be used for this positioning. During this adjustment the other beam need not be blocked. After one beam was positioned, the other beam would be positioned similarly, first focusing it so it appeared to be nearly co-linear with the first beam. After each beam had been positioned so that the signal on the optical axis was a minimum, the reference frequency for the lock-in amplifier was changed from that of

Measurement procedures

For the focused beams, two types of measurements were made. In one, the intensity of one beam was held constant, and that of the other varied by placing a polarizer between the beamsplitter and M1. This beam, beam 1, was the more intense, due to the higher reflectivity of the beamsplitter. The polarizer was also used to set the intensity of beam 1 to be the same as that of beam 2. The total intensity was varied by placing neutral density filters just in front of the beamsplitter. The optical path was not significantly affected, and re-alignment of the beams was not necessary as the neutral density filters were changed. This had been a problem when neutral density filters were used instead of the polarizer to vary the relative intensity of one beam. For both series of measurements, the fluorescence signal was measured using the power spectrum analysis program as was done for the single beam measurements.

For the defocused beams, the fluorescence was determined as a function of the intensity, with the intensity of the two beams being nearly equal, as with the second series with the focused beams.

After the two types of focusing had been characterized, their use for the reduction of scattering interferences and for spatial measurements was demonstrated. Highly scattering matrices readily clog the type of burner which was used for these studies, so an alternative was to use the scatter

from unvaporized water droplets in the low temperature H_2-Ar diffusion flame, and also, as a worst case, the scatter from water droplets with no flame. As an example of the spatial measurements, the flame was translated towards the monochromator, and away, to give a cross-section of the Na atom population across the width of the flame. Both focused and defocused beams were used. The relative fluorescence signal at the sum frequency f_1+f_2 was recorded using the lock-in amplifier.

CHAPTER FOUR
RESULTS AND DISCUSSION

All power spectra plotted are averages of 16 1024 point transforms as indicated in Chapter 3 and Appendix C, with a resolution of 2 Hz. This corresponds to a two-second time series. The ordinate for the linear plots is scaled proportional to rms amplitude/$Hz^{1/2}$ while that for the semi-log plots is the power spectral density, amplitude^2/Hz, in decibels. The linear plots are useful for qualitative comparison of signal levels, i.e., signals of similar order of magnitude. The semi-log plots reveal more of the fine detail of the spectral composition of the modulated signal and gives a better understanding of the interactions.

Single-Beam Modulation

Typical power spectra for square-wave modulation are given in Figures 4-1 and 4-2. The magnitude of the fundamental, the second and the third harmonic are plotted versus the measured power in Figure 4-3. The signals plotted are taken from the print-out of the power spectra and correspond to the peak value with the baseline subtracted. Similar results are obtained by integrating the data corresponding to the given peak.

Figure 4-1. Typical flame fluorescence power spectrum for 1 ppm Na, with single beam focused at high power (425 mW). Chopper frequency 280 Hz.

a) Linear plot
b) Semi-log plot

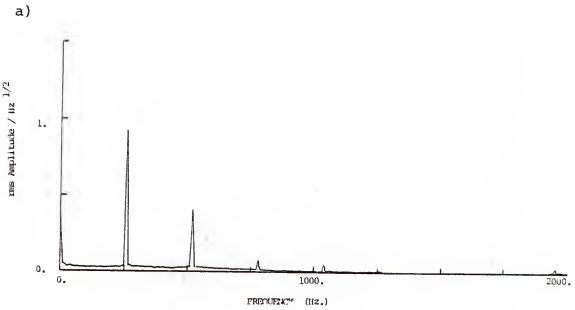
a)
rms Amplitude / Hz 1/2
1.
0.
0.
1000.
2000.
FREQUENCY (Hz.)

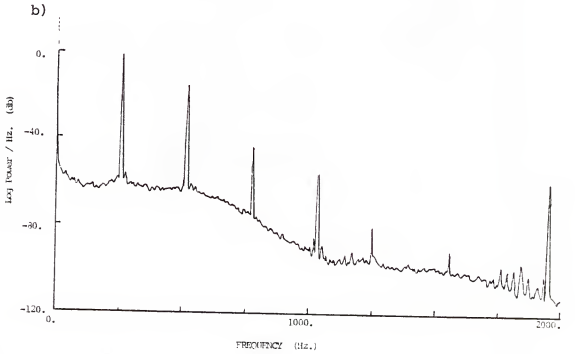
b)
0.
-40.
-80.
-120.
Log (PSD) / Hz. (dB)
0.
1000.
2000.
FREQUENCY (Hz.)

Figure 4-2. Typical power spectrum for fluorescence, 1 ppm Na, single beam, square-wave modulated, focused at lowpower (3.5 mW)

a) Linear plot
b) Semi-log plot. Second harmonic is significantly reduced compared to Fig 4.1

a)

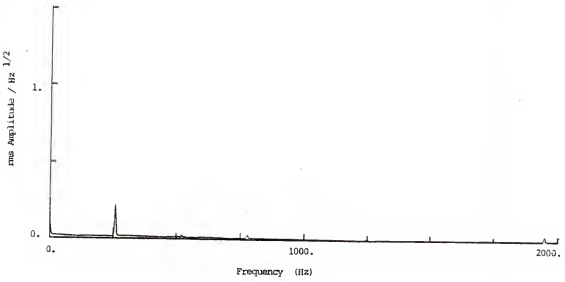
rms Amplitude / Hz 1/2
1.
0.
0.
1000.
2000.
Frequency (Hz)

b)

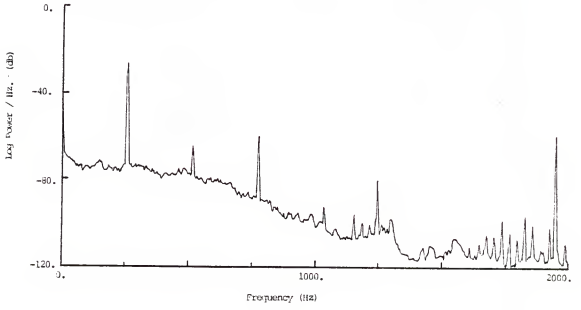
0.
-40.
-80.
-120.
Log Power / Hz. (db)
0.
1000.
2000.
Frequency (Hz)

Figure 4-3. Fluorescence signal at the fundamental, second and third harmonics vs laser power. Single focused beam, square-wave modulated.

● Fundamental
■ Second harmonic
▲ Third harmonic

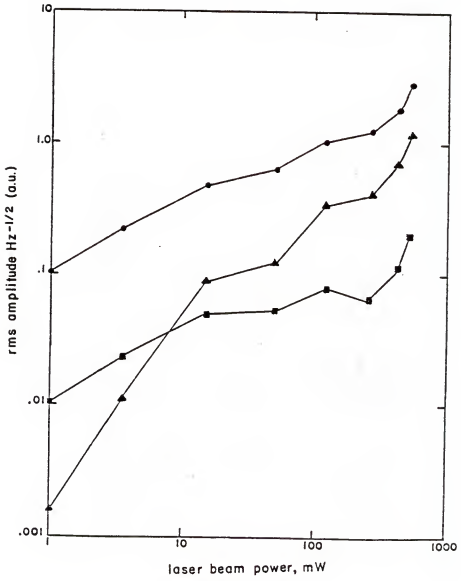
10
1.0
.1
.01
.001
rms amplitude Hz-1/2 (a.u.)
1
10
100
1000
laser beam power, mW

The magnitude of the second harmonic was unexpected. Since the square of a square wave is another square wave, it might be expected that the two would have the same frequency content. Freuholz and Gelbwachs (13) found a fundamental to second-harmonic ratio of about 6 for square-wave modulation with intensities between 3 and 7 kW/cm^2. Here the ratio is about 3. From the first-order approximation for square-wave modulation, a factor similar to Freuholz's would be expected. By examining the Fourier series expansion of a square wave, Eqn. 2.13, and the square thereof,

$$f(t)^2 = \frac{4}{\pi^2}\left(\cos\omega t - \frac{1}{3}\cos 3\omega t + \frac{1}{5}\cos 5\omega t \ \ldots\right)^2$$

one can see the origin of a second-harmonic component, from the identity $\cos^2 A = (1+\cos 2A)/2$.

The shape of the curve is typical of saturation curves where the laser beam is focused to a spot that is small compared to the flame thickness. Only where the spatial distribution of the laser irradiance is uniform in the observed part of the flame is a plateau found as in Fig. 2-1b (24). It should be noted that the point corresponding to the highest power, 520 mW average (with chopper in place) or 1.04 W peak, was the only one with no polarizer in the beam path, so the spatial distribution might have been somewhat different.

Single-beam modulation has the advantages of requiring fewer optical components and having less critical adjustments. Spatial resolution is determined by the volume of the atom cell that is saturated plus the projection of that upon the monochromator entrance slit. Thus optical alignment may be critical if spatial information is desired. The magnitude of the second harmonic will be considered in the evaluation of the two-beam system, to compare the effectiveness of harmonic mixing versus intermodulation.

Double-Beam Modulation

Tightly-Focused Beams

The complexity of the intermodulation power spectrum is shown in Figure 4-4 where the major intermodulation products are labeled. Figure 4-5 gives two typical power spectra for the double-beam measurement. In this first series of measurements, the intensity of beam 2 (passing through chopper 2) was held constant and the intensity of beam 1 was attenuated, so that it varied from almost twice the other to almost complete extinction. The peak intensity of beam 1 was nominally 320 mW. The results are shown in Fig. 4-6. The signal at f_1+f_2 is maximal closer to 240 mW which may be attributed to imperfect matching of the two beams; the ratio of the fundamental signals (f_1/f_2) were 1.15 and 1.08 with 320 mW and 240 mW excitation, indicating there was a closer match in intersecting intensities at the 240 mW level. This

Figure 4-4.Log power spectrum of square-wave intermodulated fluorescence showing multiple intermodulation product frequencies.

f_1 = fundamental frequency of chopper 1

f_2 = fundamental frequency of chopper 2

log power / Hz (db)
0
-100
0
1000
2000
frequency, Hz
$f_2 - f_1$
f_1
$2f_1$
$3f_1 - f_2$
$f_1 + f_2$
$2f_2$
$3f_1$
$2f_1 + f_2$
$3f_2 - f_1$
$4f_1$
$3f_2$
$3f_1 + f_2$
$5f_1$
$4f_2$
$6f_1$

Figure 4-5. Power spectra of intermodulated flame fluorescence signal for tightly-focused beams; Beam 2, 320 mW
a) Beam 1, high intensity
b) Beam 2, low intensity

a)

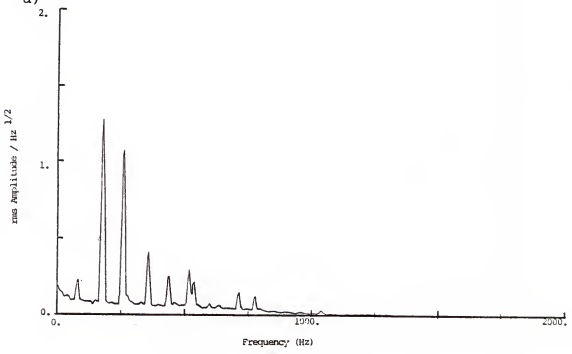
2.
1.
0.
rms Amplitude / Hz 1/2
0.
1000.
2000.
Frequency (Hz)

b)

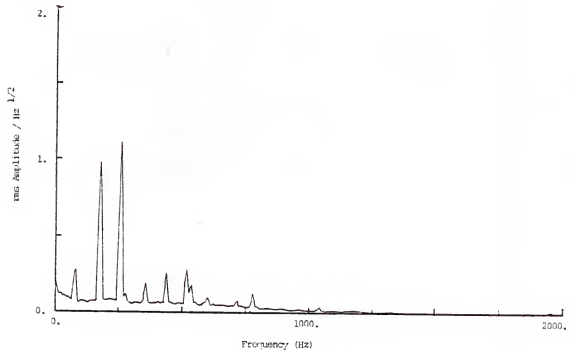
2.
1.
0.
rms Amplitude / Hz 1/2
0.
1000.
2000.
Frequency (Hz)

Figure 4-6. Comparison of second-harmonic and sum frequency signals with square-wave modulation and tightly-focused beams. Intensity of one beam held constant. (320 mW)

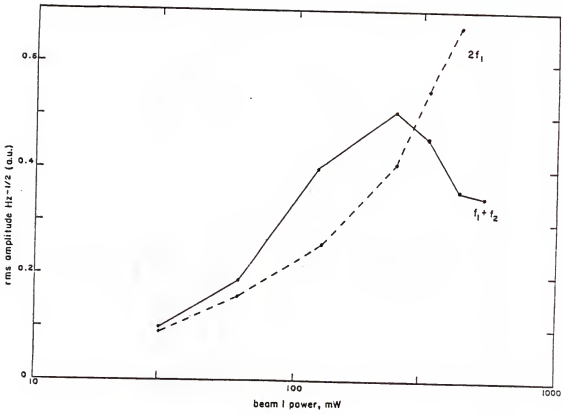
0.6
0.4
0.2
0
rms amplitude Hz$^{-1/2}$ (a.u.)
$2f_1$
$f_1 + f_2$
10
100
1000
beam 1 power, mW

curve indicates there is an optimum for the relative intensities of the two beams, as expected from theory (Eqn. 2.18), and that experimentally, approximately equal intensities are required for the highest intermodulation signal.

Since the signal at $2*f_1$ is expected to be a function of the square of I_1 while the signal at (f_1+f_2) is a function of I_1*I_2, with I_2 being held constant, it is not surprising that the second harmonic component becomes larger than the intermodulation signal as I_1 becomes larger than I_2. There appears to be less than a factor of two difference between the second harmonic and the intermodulation signal. The single-beam signal might very well be larger than that from the dual-beam system, as the laser beam is not split, nor suffer the losses from the additional optical components. Thus, square-wave modulated harmonic saturation spectroscopy should be comparable with the double-beam intermodulated spectroscopy. It, however, has limited potential for spatial resolution.

Defocused Beams

The differences between the intermodulation and harmonic products for the focused and defocused beams are shown in Figs. 4-7 and 4-8. The tightly-focused, intersecting beams have a high second-harmonic content, which is to be expected from the single-beam results. Since the volume viewed by the monochromator is much larger than the intersection

Figure 4-7. Comparison of intermodulation signals from beams tightly focused at intersection volume and defocused at intersection volume. Laser power 360 mW. Linear power spectra.
a) Tightly-focused beams, gain of 200
b) Defocused beams, gain of 20

a)

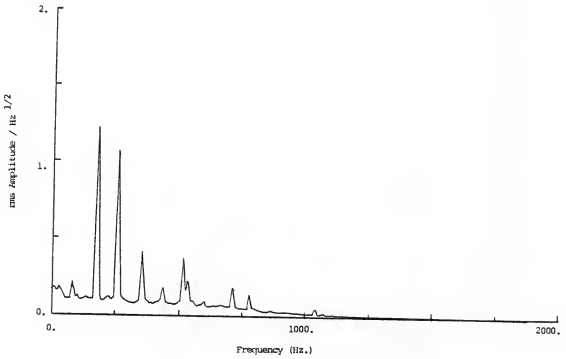
2.
1.
0.
rms Amplitude / Hz 1/2
0.
1000.
2000.
Frequency (Hz.)

b)

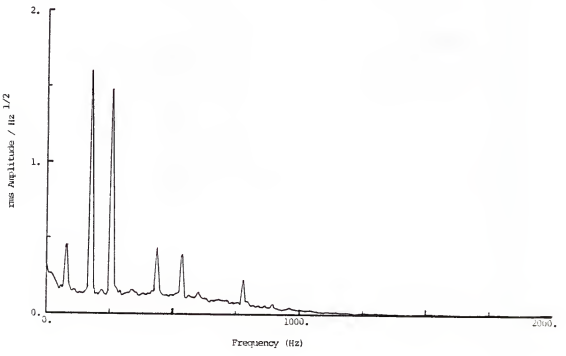
2.
1.
0.
rms Amplitude / Hz 1/2
0.
1000.
2000.
Frequency (Hz)

Figure 4-8. Comparison of intermodulation signals from beams tightly focused at intersection volume and defocused at intersection volume. Laser power 360 mW. Semi-log plot of power spectra.
a) Tightly-focused beams, gain of 200
b) Defocused beams, gain of 20

a)

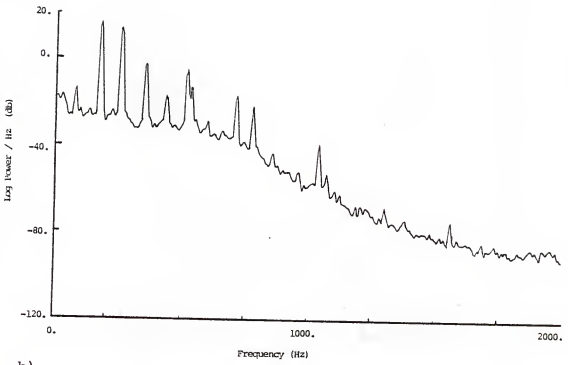
20.
0.
-40.
-80.
-120.
Log Power / Hz (db)
0.
1000.
2000.
Frequency (Hz)

b)

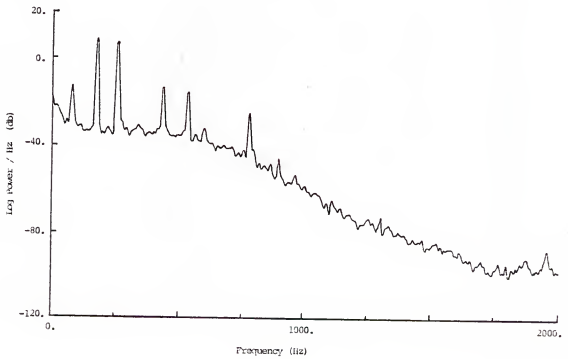
20.
0.
-40.
-80.
-120.
Log Power / Hz (db)
0.
1000.
2000.
Frequency (Hz)

volume of the two beams in the case of the tightly-focused beams, Fig. 4-7a, it is not surprising that, in this case, the single-beam components, e.g., signals at f_1 and $2f_1$, are large compared to the intermodulation signal at f_1+f_2. For the defocused case, the signal levels of the fundamental are generally 5-10 times larger than those with the tightly-focused beams at the same power levels, due in part to the larger illuminated volume. With the defocused beams, the second harmonic signal is not discernible, and the intermodulation is relatively large compared to the focused double-beam intermodulation signals.

The effect of varying the laser power for the defocused beams is shown by Fig. 4-9, where the power of the two beams is nominally the same. The fundamental frequency component is leveling off with increasing power while the intermodulation product continues to increase. Thus, for high resolution, one could use the two focused beams, while for good scattering rejection, one would get larger signals and average over a greater volume using the defocused beams.

Scattering Rejection

The effectiveness of the intermodulation in reducing scatter is shown in Figs. 4-10 and 4-11, where the power spectrum for scatter are plotted, for scatter from water droplets in a H_2-Ar diffusion flame (no O_2) and from water droplets with no flame. In neither case is there any component at the sum or difference frequencies $f_1+/-f_2$. The

Figure 4-9. Fluorescence signal at fundamental and sum frequency for two-beam square-wave modulation. Beams nearly equal intensity and defocused at point of intersection; total power varied.

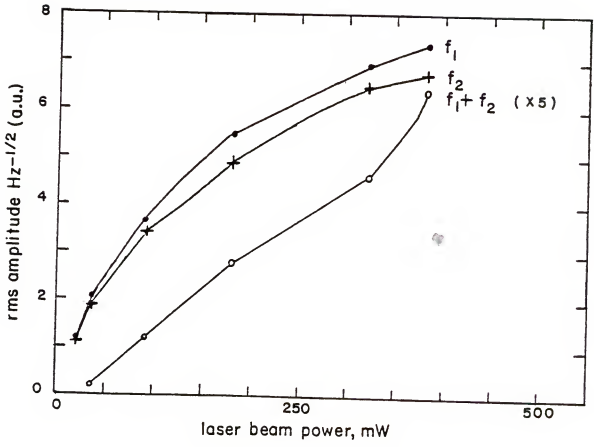
8
6
4
2
0
0
250
500
rms amplitude Hz$^{-1/2}$ (a.u.)
laser beam power, mW
f_1
f_2
$f_1 + f_2$ (x5)

Figure 4-10. Power spectrum for scatter from water aspirated in H_2-Ar diffusion flame. Gain = 20, two defocused beams, 360 mW each.

a) linear plot
b) semi-log plot

a)

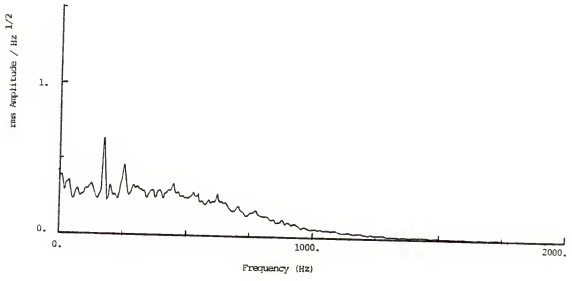
rms Amplitude / Hz 1/2
1.
0.
0.
1000.
2000.
Frequency (Hz)

b)

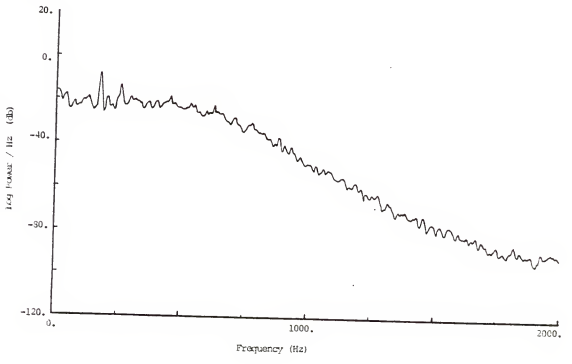
20.
0.
-40.
-80.
-120.
0.
1000.
2000.
Frequency (Hz)

Figure 4-11. Power spectrum for scatter from water aspirated with flame off. Gain = 10 , two defocused beams, 360 mW each

a) linear plot
b) semi-log plot

a)

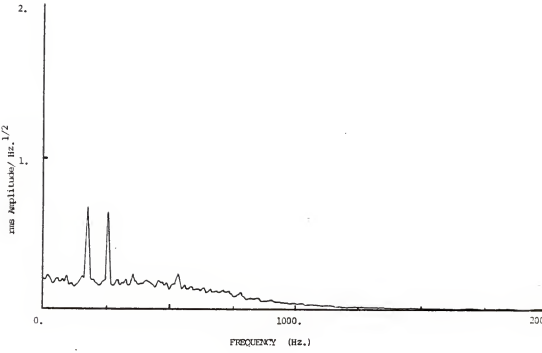
2.
1.
rms Amplitude/ Hz.1/2
0.
1000.
2000.
FREQUENCY (Hz.)

b)

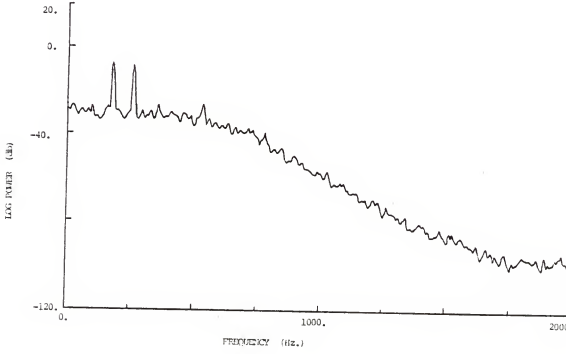
20.
0.
-40.
-120.
LOG POWER (dB)
0.
1000.
2000.
FREQUENCY (Hz.)

shot noise from the large scatter signal gives the nearly uniform density out to about 700 Hz, the cut-off frequency of the Butterworth filter. The roll-off of this white noise power spectrum indicates that signals above 1.5 kHz are attenuated by a factor of at least 10^{-3} (60 db).

The reduction in the scattering signal may be shown more clearly in the time domain, comparing lock-in amplifier output signals at the fundamental frequency and at the intermodulation frequency, as in Fig. 4-12. This represents a significant reduction in the scatter signal and indicates the potential of using intermodulation saturation spectroscopy for the reduction of scatter interferences.

Spatial Resolution

As an example of the use of the intermodulation signal for spatial resolution, the Na atom density in the flame was mapped by translating the flame towards the monochromator and back to get the distribution across the flame width. The flame was moved in approximately 1 mm steps. The length of the volume element measured was determined by either the volume in which intermodulation saturation was occurring, or by the 2 mm slit height (slit oriented parallel to the beam), whichever was smaller. The profile was measured with the focused beams, and also the defocused beams. The defocused beams gave approximately 10 times larger a signal, and had better signal/noise ratio, but either was adequate for this purpose. The scan across the flame shown in Fig. 4-13

Figure 4-12. Recorder tracing of scatter signal, defocused square-wave modulated beams, 360 mW each

a) Hydrogen diffusion flame, as in Fig. 4-10, lock-in amplifier reference frequency f_1
b) as in a, f_1+f_2 reference frequency
c) argon + water droplets, as in 4-11. Signal measured at f_1.
d) as in c, signal measured at f_1+f_2

a

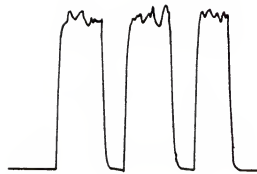

b

c

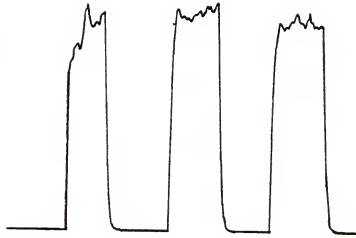

d

Figure 4-13. Sodium atom distribution across width of flame; 1 ppm Na in H_2-O_2-Ar flame.

a) Schematic diagram; burner moved along optical axis of monochromator, ~ 1 mm between observations

b) Intermodulated fluorescence signal measured with lock-in amplifier reference frequency of f_1+f_2, using defocused, nearly co-linear, intersecting beams

a)

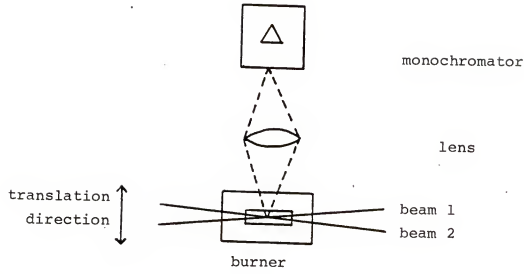
monochromator
lens
translation
direction
beam 1
beam 2
burner

b)

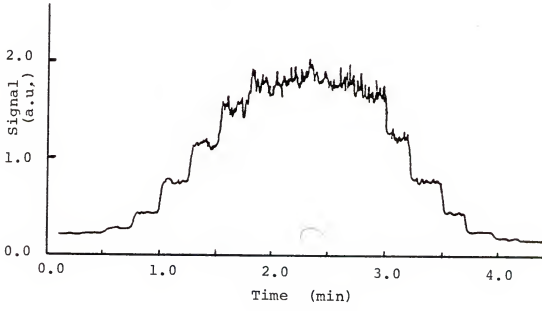
2.0
1.0
0.0
Signal (a.u.)
0.0
1.0
2.0
3.0
4.0
Time (min)

gives the relative Na atom distribution 2 cm above the top of the burner head, under the flame conditions used in this study.

CHAPTER FIVE
CONCLUSIONS

The intermodulation component of the fluorescence signal in atomic fluorescence may be a significant fraction of the saturation signal. By using two beams modulated at different frequencies, a resultant sum or difference frequency may be selected to avoid frequency regions with high noise components. Harmonic saturation spectroscopy is a special case of intermodulated saturation spectroscopy in which the frequency and position of the two beams are the same. The same theoretical considerations apply in determining the modulation products.

The use of intermodulated atomic fluorescence for the reduction of scattering and for spatial resolution has been demonstrated using Na in a H_2-O_2-Ar flame. If saturation can be achieved, the signal/noise ratio may be improved by defocusing the beams and illuminating a larger volume. If fine spatial resolution is required, the beams may be tightly focused using short focal length lenses. Sodium has been used extensively as a seed for studies of flame chemistry. It is of interest for flame diagnostics, combustion diagnostics, and as a model from which techniques have been developed for the stuay of radicals in combustion processes, as well as for physical studies.

Further application of intermodulated flame fluorescence would require the use of lasers which can saturate other elements of analytical interest. Pulsed dye lasers have much higher peak powers and cover a wider range of wavelengths. For such devices, a suitable modulation/detection scheme would need to be developed, probably somewhat more elaborate than the preamplifier and phase-sensitive amplifier or analog-to-digital converter used here for the modulated cw dye laser.

APPENDIX A
CIRCUITS FOR INTERMODULATION MEASUREMENTS

Lock-in Amplifier Reference Circuit

The circuit shown in Fig. A-1 was constructed to generate a signal that could be used as the reference waveform for the intermodulation signal. Input and output waveforms are shown in Fig. A-2. The power spectra of the ouptputs are shown in Figs. A-3 and 4. The exclusive-OR circuit generates only the sum and difference frequencies (and other higher frequency components of those waveforms). Thus, the requirements for a frequency selective amplifier to give a single frequency output are not so demanding, using this configuration. Schmitt trigger gates were used as the chopper reference signals are not necessarily TTL compatible. The operational amplifiers are used in a non-inverting voltage-follower configuration as output buffers for analog signals. A frequency-selective amplifier (PAR 210) was used to select a particular frequency component of the output waveform, and to generate a bipolar sine wave which was used as the reference signal for the lock-in.

The alternate output, from the NAND gates, was used for test purposes as it simulates the fluorescence signal in the case of complete saturation.

Figure A-1. Lock-in reference circuit.

U1 -	74LS132	Schmitt trigger NAND Gate
U2 -	74LS86	Exclusive OR gate
U3 -	74LS00	NAND gate
U4 -	LM358	Dual Operational Amplifier

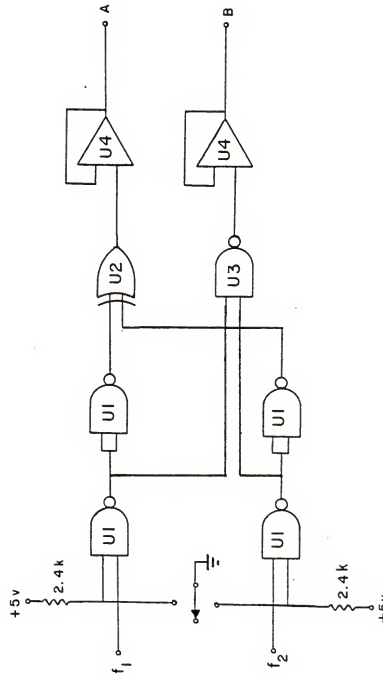
A
B
U4
U4
U2
U3
U1
U1
U1
U1
+5v
2.4k
2.4k
+5v
f_1
f_2

Figure A-2. Lock-in amplifier reference circuit waveforms.
a) Reference 1 waveform, f_1
b) Reference 2 waveform, f_2
c) NAND gate output, B
d) Exclusive OR output, A

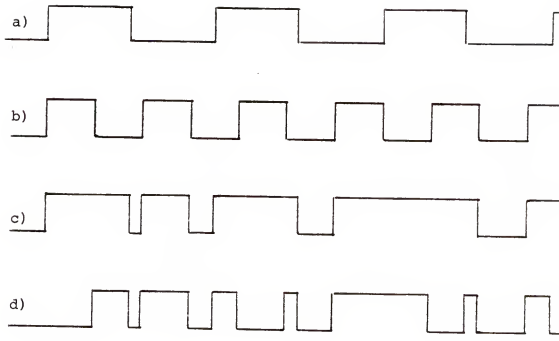
a)
b)
c)
d)

Figure A-3. Power spectrum of exclusive OR reference output waveform
a) Linear plot
b) Semi-log plot

a)

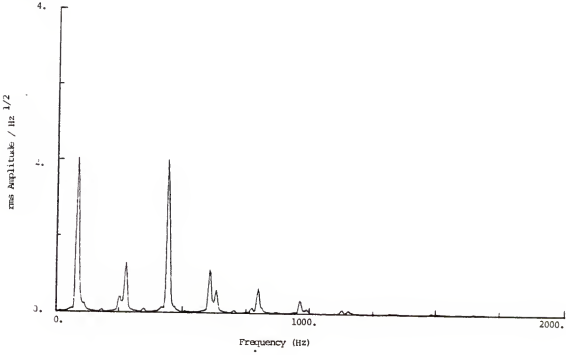
4.
0.
1000.
2000.
rms Amplitude / Hz 1/2
Frequency (Hz)

b)

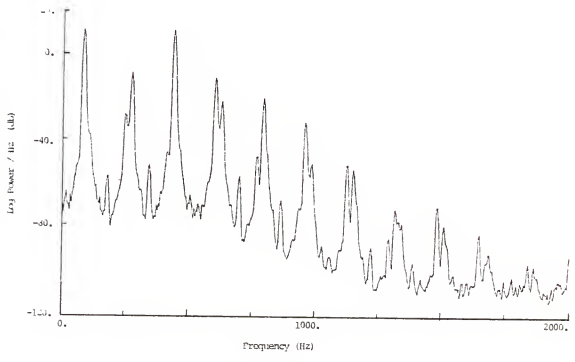
0.
-40.
-80.
0.
1000.
2000.
Frequency (Hz)

Figure A-4. Power spectrum of NAND gate reference output waveform
a) Linear plot
b) Semi-log plot

a)

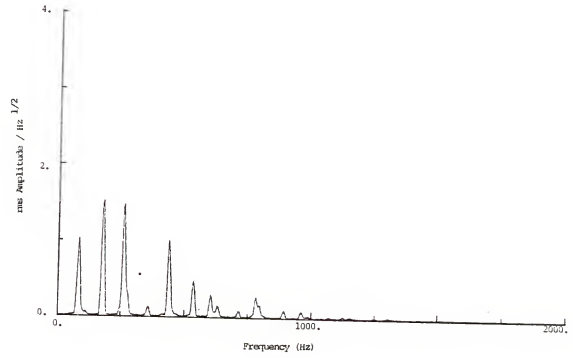
4.
2.
0.
0.
1000.
2000.
rms Amplitude / Hz 1/2
Frequency (Hz)

b)

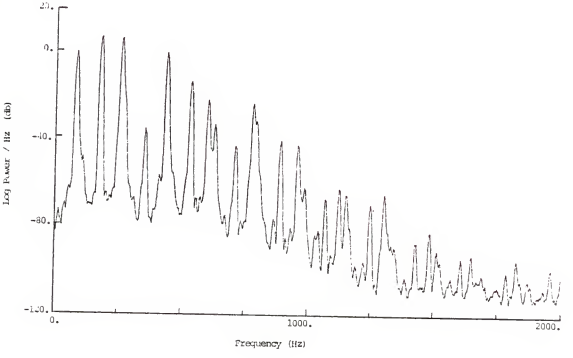
20.
0.
-40.
-80.
-120.
0.
1000.
2000.
Log Power / Hz (dB)
Frequency (Hz)

Anti-aliasing Filter

A low-pass filter was constructed to prevent aliasing, i.e., higher frequency signals appearing at lower frequencies, with the FFT. In order to obtain a sharp cutoff, a fourth-order Butterworth filter was constructed using a digital switched-capacitor filter (National MF10). The Butterworth filter has maximally flat amplitude response in the passband, though it has a non-linear phase characteristic which results in over-shoot in the time domain (19), but this was not considered significant for the measurement of power spectra.

The ratios R2A/R2B and R3A/R3B, which determine the filter characteristics, were obtained by trimming available components to give the desired frequency response. The resistors R01 and R02 were selected to give minimum DC offset of the internal amplifiers, and thus maintain maximum dynamic range. The overall voltage gain was approximately one for signals within the pass-band. The maximum input voltage should be less than 5.6 Vp-p for this design, according to the manufacturer's application notes. Since the A/D converter with which this filter was used had a range of +/- 1 V, the input signal was kept less than 2 Vp-p.

This switched-capacitor filter building block uses an external clock to set the cutoff frequency, which makes it quite versatile for use with the FFT for power spectrum analysis. Analog filters, especially higher-order filters,

Figure A-5. Anti-aliasing filter circuit
U1 - TL072 Operational amplifier
U2 - MF10 Switched-capacitor filter chip
R3A/R2A = 1.848
R3B/R2B = 0.765
R0A, R0B offset zero trim

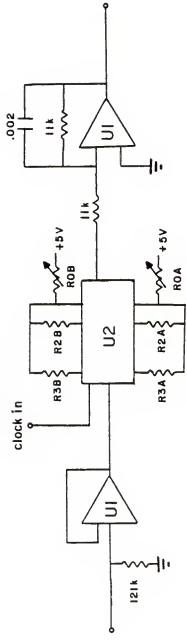
.002
11k
U1
11k
+5V
ROB
+5V
ROA
R2B
U2
R2A
R3B
R3A
clock in
U1
121k

require several precisely matched components for each choice of frequencies. This filter requires precise matching only of the resistors to establish the filter characteristics, and then a signal generator can be used to vary the cutoff frequency.

The amplitude response was checked using a signal generator as an input and determining the amount of attenuation. In order to have minimal attenuation over the frequency range of interest, a cutoff frequency of 700 Hz was selected. This gave a 2% attenuation at 500 Hz. The active low-pass filter at the output reduces some of the clock and switching noise which is characteristic of this type of device. It also acts as a buffer amplifier to avoid any loading effects on the filter output.

APPENDIX B
ESTIMATION OF POWER SPECTRA

The frequency components of the fluorescence signal were determined by estimating the power spectra using the FFT. The program was based on one recommmended by a Digital Signal Processing Committee of the IEEE Acoustics, Speech and Signal Processing Society (25). They had tested the program on various computers, including a DEC PDP 11/34A similar to the one used here, and found it suitable to recommend for use. The modifications made here did not involve changing the algorithm, but only the input and output for use with this real-time data acquisition system.

The program is based on the modified periodogram method of Welch (26), which is computationally efficient and gives good results (27). The periodogram is a measure of the rms amplitude of a short data record. The periodogram is modified through the use of a window, which compensates for the finite data record and reduces side-lobes on the resultant periodogram (28), as shown in Figs. B-1 and B-2. A number of modified periodograms are averaged to give an estimate of the power spectrum. Several other FFT subroutines from the same reference were evaluated to speed the data analysis (4 seconds for a 1024 point complex transform). No significant improvement (less than a factor of two, accompanied by heavy

Figure B-1. Power spectrum of sine wave input. Rectangular window, otherwise same conditions as experimental measurements
a) linear plot
b) semi-log plot

a)

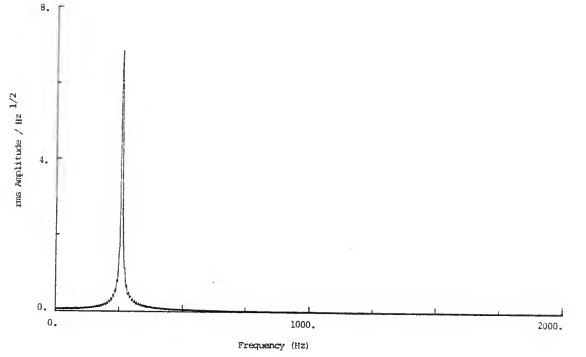
8.
4.
0.
rms Amplitude / Hz 1/2
0.
1000.
2000.
Frequency (Hz)

b)

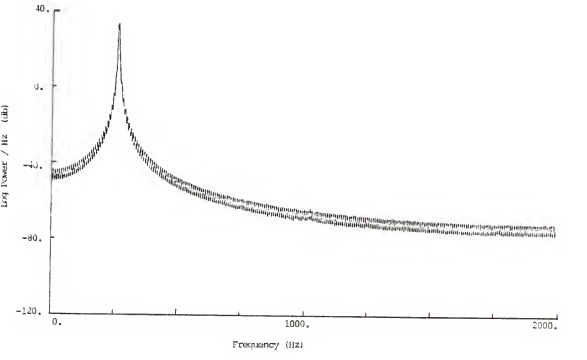
40.
0.
-40.
-80.
-120.
Log Power / Hz (db)
0.
1000.
2000.
Frequency (Hz)

Figure B-2. Power spectrum of sine wave input. Hamming window; same conditions as experimental measurements.

a) linear plot
b) semi-log plot

a)

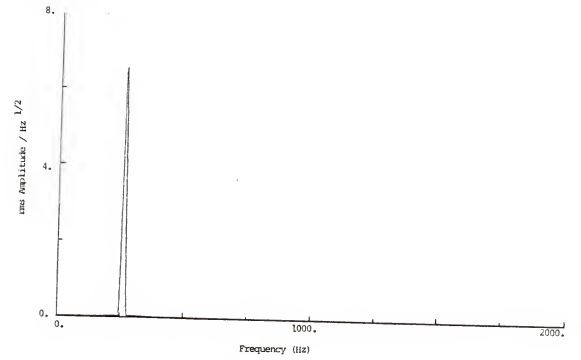
8.
4.
0.
rms Amplitude / Hz 1/2
0.
1000.
2000.
Frequency (Hz)

b)

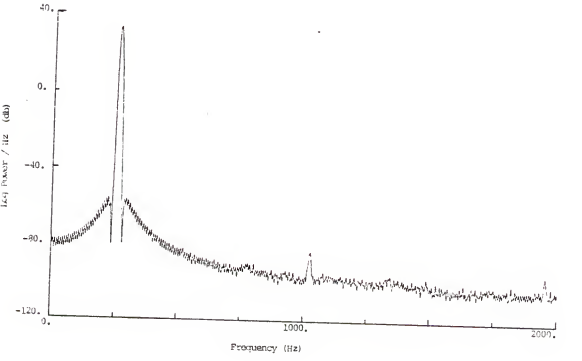
40.
0.
-40.
-80.
-120.
Log Power / Hz (dB)
0.
1000.
2000.
Frequency (Hz)

utilization of storage) was obtained with floating point routines. The integer routine in the DEC Lab Applications Package was a factor of four faster but was not compatible with the use of a window for the data.

The A/D subroutine (originally written by D.L. Bolton and modified for use under the TSX operating system) could acquire data at a rate up to 44 kHz. The maximum length record was 8192 (8 k) data points, due to the size of the Fortran I/O package. A number of 8 k records could be stored on disc and subsequently analyzed with the power spectrum analysis program. Results could be plotted on a video graphics terminal (DEC VT100 with Matrox GT-600 graphics) or with a digital plotter (Houston Instruments DMP-4). A graphics subroutine package from the DEC Users Group (SFGL70) was used for the video plotting. A set of subroutines (HIPLIB) written by D.L. Bolton (29) was used for the hard-copy output.

REFERENCES

1. N. Omenetto, Editor, Analytical Laser Spectroscopy, John Wiley and Sons, New York, 1979.

2. D.R. Crosley, Editor, Laser Probes for Combustion Chemistry, American Chemical Society, Washington, D.C., 1980.

3. J.H. Bechtel and A.R. Chraplyvy, Proc. IEEE 70, 659 (1982).

4. R.F. Alfano, Editor, Biological Events Probed by Ultrafast Laser Spectroscopy, Academic Press, New York, 1982.

5. C.Th.J. Alkemade, Appl. Spectrosc. 35, 1 (1981).

6. J.A. Gelbwachs, C.F. Klein, and J.E. Wessel, Appl. Phys. Lett. 30, 489 (1977).

7. R.P. Lucht, D.W. Sweeney, and N.M. Laurendeau, Combust. Flame 50, 189 (1983).

8. J.W. Daily, Appl. Opt. 17, 1610 (1978).

9. N. Omenetto, L.P. Hart, and J.D. Winefordner, Appl. Spectrosc. 26, 612 (1972).

10. D.A. Goff and E.S. Yeung, Anal. Chem. 50, 625 (1978).

11. C.Th.J. Alkemade, "To Catch a Single Atom," presented at the 6th FACSS Meeting, Philadelphia, PA., 17 Sept. 1979.

12. M.S.Sorem and A.L. Schawlow, Opt. Comm. 5, 148 (1972).

13. R.P. Freuholz and J.A. Gelbwachs, Appl. Opt. 19, 2735 (1980).

14. C.Th.J. Alkemade, Tj. Hollander, W. Snellman, and P.J.Th. Zeegers, Metal Vapours in Flames, Pergamon Press, Oxford, 1982.

15. K. Shimoda, Editor, High Resolution Laser Spectroscopy, Springer-Verlag, Berlin, 1976.

16. V.S. Letokhof, Nonlinear Laser Chemistry, Springer-Verlag, Berlin, 1983.

17. J.W. Daily, Appl. Opt. 16, 2322 (1977).

18. I.S.Gradshteyn and I.M. Rhyzhik, Table of Integrals, Series, and Products, Academic Press, New York, 1974.

19. C.D. McGillem and G.R. Cooper, Continuous and Discrete Signal and System Analysis, Holt, Rinehart, Winston, Inc., New York, 1974.

20. A. Corney, Atomic and Laser Spectroscopy, Clarendon Press, Oxford, 1977.

21. A.P. Thorne, Spectrophysics, Chapman and Hall, London, 1974.

22. W. Demtroeder, Laser Spectroscopy, Springer-Verlag, Berlin, 1982.

23. R.A. van Calcar, M.J.M. van de Ven, B.K. van Uitert, K.J. Bienwenga, Tj. Hollander and C.Th.J. Alkemade, J. Quant. Spectrosc. Radiat. Transfer 21, 11 (1979).

24. M.L. Elder, C.A. van Dijk, J.D. Winefordner, Spectrochim. Acta 38B, 1183 (1983).

25. L.R. Rabiner, R.W. Schafer and D. Dlugos, Programs for Digital Signal Processing, Digital Signal Processing Committee, IEEE Acoustics, Speech and Signal Processing Society, Eds., IEEE Press, New York, 1979.

26. P.D. Welch, IEEE Trans. on Audio and Electroacoustics, AU-15, 70 (1967).

27. A. Peled and B. Liu, Digital Signal Processing Theory, Design and Implementation, John Wiley and Sons, New York, 1976.

28. R.B. Blackman and J.W. Tukey, The Measurement of Power Spectra, Dover Publishers, New York, 1959.

29. D.L. Bolton, Laser Excited Site Selection Spectroscopy for the Selective Determination of Organic Species, Ph.D. Dissertation, University of Florida, (1983).

BIOGRAPHICAL SKETCH

Lucas P. Hart, III, was born 23 January 1943 at Pittsfield, Massachusetts. He attended public schools in Pittsfield and in Glens Falls New York. He attended Swarthmore College in Swarthmore, Pennsylvania, and received a Bachelor of Arts degree, in chemistry. In 1965, he entered the University of Florida. After serving two years as a graduate teaching assistant in the Chemistry Department, he served as a graduate research assistant in the Analytical Division, working for Dr. J. D. Winefordner. He received a Master of Science degree in 1972, and continued to work for Dr. Winefordner as a research associate and again as a graduate research assistant. He then worked for four years as a research specialist for the General Electric Company, Capacitor Products Department, in Hudson Falls, New York. In 1982, he returned to the University of Florida to complete the requirements for his doctorate.

I certify that I have read this study and that in my opinion it conforms to acceptable standards of scholarly presentation and is fully adequate, in scope and quality, as a dissertation for the degree of Doctor of Philosophy.

James D. Winefordner, Chairman
Graduate Research Professor of
Chemistry

I certify that I have read this study and that in my opinion it conforms to acceptable standards of scholarly presentation and is fully adequate, in scope and quality, as a dissertation for the degree of Doctor of Philosophy.

John E. Singley
Professor of Environmental
Engineering Sciences

I certify that I have read this study and that in my opinion it conforms to acceptable standards of scholarly presentation and is fully adequate, in scope and quality, as a dissertation for the degree of Doctor of Philosophy.

John G. Dorsey
Assistant Professor of Chemistry

This dissertation was submitted to the Graduate Faculty of the Department of Chemistry in the College of Liberal Arts and Sciences and to the Graduate School, and was accepted as partial fulfillment of the requirements for the degree of Doctor of Philosophy.

April 1984

Dean for Graduate Studies
and Research